Low-Complexity PAPR Reduction Scheme Without Side Information for OFDM Systems

Seung-Sik Eom, *Student Member, IEEE*, Haewoon Nam, *Senior Member, IEEE*, and Young-Chai Ko, *Senior Member, IEEE*

***Abstract*—This paper proposes a novel peak to average power ratio (PAPR) reduction scheme that requires no side information in orthogonal frequency division multiplexing (OFDM) systems. Unlike the selective mapping (SLM) or the partial transmit sequence (PTS) scheme, the proposed scheme deals with post inverse fast Fourier transform (IFFT) symbols and thus requires only a single IFFT processor in the transmitter. Compared to other conventional schemes implemented with a single IFFT processor, such as the circularly shifted phase sequences (CSPS) or the optimised circularly shifted phase sequences (OCSPS) method, the proposed scheme achieves an even lower complexity since only phase rotation and cyclic shifting of OFDM symbols are performed. More importantly, the proposed scheme significantly outperforms the CSPS and the OCSPS methods in reducing PAPR as shown in simulation results. An added benefit of the proposed scheme is that it employs a linear receiver, such as a maximal likelihood (ML) detector, a minimum mean square error (MMSE) estimator, or a zero forcing (ZF) estimator, to demap quadrature amplitude modulation (QAM) symbols. Especially the ML detector demaps the QAM symbols with no side information. Simulation results also show that the bit error rate (BER) of the proposed scheme has no loss when the ML detector, the ZF or the MMSE estimator is used with hard-decision compared to that of the conventional OFDM system without any PAPR reduction scheme over Rayleigh fading channel.**

***Index Terms*—Circularly shifted phase sequences (CSPS), complementary cumulative distribution function (CCDF), optimized circularly shifted phase sequences (OCSPS), orthogonal frequency division multiplexing (OFDM), partial transmit sequence scheme (PTS), peak-to-average power ratio (PAPR), time-domain processing.**

Manuscript received June 16, 2011; revised November 17, 2011 and March 06, 2012; accepted March 06, 2012. Date of publication March 23, 2012; date of current version June 12, 2012. The associate editor coordinating the review of this manuscript and approving it for publication was Prof. Sofiene Affes. This work was supported by the The Ministry of Knowledge Economy (MKE), Korea, under the Information Technology Research Center (ITRC) support program supervised by the National IT Industry Promotion Agency (NIPA) [NIPA-2012-(H0301-12-1003)] and in part by Korea University. This research was also supported by Basic Science Research Program through the National Research Foundation of Korea (NRF) funded by the Ministry of Education, Science and Technology (NRF-2012-0012522). This paper was presented in part at the IEEE International Conference on Communications (ICC), Kyoto, Japan, June 2011.

S.-S. Eom, and Y.-C. Ko are with the School of Electrical Engineering, Korea University, Seoul 136-713, Korea (e-mail: drdja@korea.ac.kr; koyc@korea.ac.kr).

H. Nam is with the Department of Electronics and Communication Engineering, Hanyang University, Ansan, 426-791, Korea (e-mail: hnam@hanyang.ac.kr)

Color versions of one or more of the figures in this paper are available online at http://ieeexplore.ieee.org.

Digital Object Identifier 10.1109/TSP.2012.2191779

I. Introduction

ORTHOGONAL FREQUENCY DIVISION MULTIPLEXING (OFDM) has recently been widely adopted in various wireless communication standards, such as terrestrial digital video broadcasting (DVB-T) and wireless local area network (WLAN), thanks to high spectral efficiency and robustness especially in a frequency selective channel environment [1]–[3]. Because of the inherent Fourier transform operation, where numerous sinusoidal waves of different frequencies and phases are constructively or destructively added, the output signal fluctuates with high peak-to-average power ratio (PAPR), which requires the transmitter to use a linear high power amplifier (HPA) with a wide linear region so as to avoid the output signal distortion [4].

Many PAPR reduction schemes have been proposed during the last decades, where most of them achieve a reduced PAPR at the expense of a high computational complexity or an explicit transmission of side information (SI). Among those are amplitude clipping [5], [6], coding based schemes [7]–[9], tone reservation (TR) [10], tone injection (TI) [10], active constellation extension (ACE) [11], selected mapping (SLM) [12] and partial transmit sequence (PTS) [13]–[18]. Note that the need of SI decreases the spectral efficiency in general when it is transmitted through a dedicated channel. In [19], Breiling *et al.* proposed a scrambling scheme which inserts several bits at the end of the data bit stream before scrambling. This scheme does not require an explicit SI transmission but the spectral efficiency is still reduced due to the inserted bits. Some PAPR reduction schemes [20], [21] do not require SI, but they are applicable only to pilot based OFDM systems.

High computational complexity is another main issue in the design of PAPR reduction schemes. The circularly shifted phase sequences (CSPS) and the optimised circularly shifted phase sequences (OCSPS) methods proposed in [22] offer a lower computational complexity than the conventional PTS scheme, while the PAPR reduction performance of those schemes is close to that of the conventional PTS scheme. Another PAPR scheme with reduced complexity is the time domain symbol combining (TDSC) scheme proposed in [23], where several post-IFFT symbols are combined in various ways and normalized in power before transmission in order to reduce PAPR by utilizing the fact that each post-IFFT symbol is independent from the other. However, the TDSC scheme has a shortcoming in that the bit error rate (BER) performance is degraded because of a varying output symbol power when combining post-IFFT symbols.

Motivated by the fact that time-domain processing of post-IFFT symbols is implemented with only a single IFFT processor, this paper proposes a novel PAPR reduction scheme performed in time domain with lower complexity. Similar to the other PAPR reduction schemes, such as CSPS and OCSPS, the proposed scheme generates a number of different representations each possibly with a different PAPR from a post-IFFT symbol to give the diversity in PAPR. The proposed scheme consists of two successive stages, which are phase rotation and cyclic shifting by an offset. More specifically, at the phase rotation stage the output symbol from IFFT is rotated in a complex constellation domain by a certain degree. Subsequently, at the cyclic shifting stage the quadrature component of the output symbol from the phase rotation stage is cyclically shifted by a certain offset, which is similar to offset-PSK (OPSK) modulation except that the offset is large and variable in the proposed scheme. We obtain the diversity in terms of PAPR by repeating the two successive stages, while changing the value of the offset, for a given times in an iterative fashion.

The intuition behind this iteration of two stages is as follows. The phase rotation of a post-IFFT symbol contributes each sample in the symbol to redistribute the power of the sample between the in-phase and quadrature components. In other words, the amplitude of the in-phase or the quadrature component can be reduced after the rotation. On the other hand, the cyclic shifting of the quadrature components of a post-IFFT symbol realigns the quadrature samples in time (in-phase components are intact). Since the average power of post-IFFT symbols does not change by the cyclic shifting, this cyclic shifting stage aims to reduce the peak power and further reduce the PAPR by separating the in-phase samples with high amplitudes and the quadrature samples with high amplitudes such that they are not aligned. This two step procedure of first reducing the amplitude of in-phase or quadrature samples and then realigning the quadrature components are done in an iterative fashion to continue reducing the PAPR effectively.

Furthermore, the proposed scheme allows the receiver to use a maximal likelihood (ML) detector to decode source symbols without SI [24], [25]. A minimum mean square error (MMSE) or a zero forcing (ZF) estimator can be used in the receiver if SI is available at the receiver. It is shown that the decoded bits by the ML detector (or by the ZF or the MMSE estimator) have no bit error rate (BER) loss compared to the BER performance of the OFDM system without any PAPR reduction scheme over Rayleigh multipath fading channel. More importantly, extensive simulations reveal that the proposed scheme offers a lower PAPR than the conventional schemes using a single IFFT such as the CSPS and the OCSPS methods.

This paper is organized as follows. Section II reviews the representation of OFDM signals and PAPR in both continuous and discrete time domains. Section III introduces the proposed scheme along with the analytical formulation of the design. The computational complexity of the proposed scheme is also compared with those of the CSPS and the OCSPS methods. Section IV provides the detailed description of the receiver structure, where the ML detector, the ZF and the MMSE estimators for the source symbols are derived. Section V presents simulation results, followed by the concluding remarks in Section VI.

II. OFDM Signals and PAPR

In OFDM system, a data block of N symbols, denoted by $\mathrm{X} = [X_0, X_1, \cdots, X_{N-1}]^{\mathsf{T}}$, is modulated by a set of orthogonal subcarriers, $\{f_k, k = 0, 1, \cdots, N-1\}$, where T denotes the transpose. In order to preserve the orthogonality, the spacing between neighboring subcarriers Δf is set to be a multiple of $\frac{1}{T}$, i.e., $\Delta f = m\frac{1}{T}$ where T is the duration of an OFDM symbol and m is a positive integer. We set m to be the least positive integer, i.e., $m = 1$, in order to make full use of the bandwidth. Then the transmitted OFDM symbol is given by

$$x(t) = \frac{1}{\sqrt{N}} \sum_{k=0}^{N-1} X_k \exp(j2\pi f_k t), \quad 0 \le t \le T. \tag{1}$$

The PAPR of the transmitted OFDM symbol is defined in continuous time domain as

$$\mathrm{PAPR} = \frac{\max_{0\le t\le T} |x(t)|^2}{\frac{1}{T}\int_0^T |x(t)|^2 \, dt}. \tag{2}$$

But since practical OFDM systems are implemented by IFFT, the PAPR is often measured in discrete time domain, where the time domain samples are assumed to be oversampled by a certain factor W[1]. Then we can define the PAPR for the sampled OFDM symbol with over-sampling factor, W, as

$$\mathrm{PAPR} = \frac{\max_{0\le n\le NW-1} |x_n|^2}{E\left[|x_n|^2\right]}. \tag{3}$$

where $E[\cdot]$ denotes expectation.

III. Proposed PAPR Reduction Scheme

The proposed scheme, similar to the CSPS and the OCSPS methods, performs time-domain processing of generating multiple candidate symbols and selects the one with the lowest PAPR.

A. Structure of the Proposed Scheme

Fig. 1 illustrates the general transmitter structure of the proposed scheme. As shown in Fig. 1(a), the output symbol of the IFFT processor is processed by multiple *in-phase and quadrature recombination* (IQRC) blocks. In each IQRC, the quadrature component with a different offset is (re)combined with the common in-phase component. Fig. 1(b) shows an IQRC block in detail, which consists of multiple subunits dubbed *joint rotation and offset* (JROF). Assume that the total number of IQRC blocks is U, where the uth IQRC is denoted by $IQRC - u$, $u = 1, \cdots, U$. Each IQRC has L JROFs, where the lth JROF is $JROF - l$, $l = 1, \cdots, L$. Including the original post-IFFT symbol, $L \times U + 1$ different representations of an OFDM symbol are generated by U IQRCs each with L JROFs. Among those $L \times U + 1$ generated symbols, the signal with the minimum peak power (or PAPR) is selected to be transmitted.

At the phase rotation stage, each time domain sample of an OFDM symbol is rotated in complex constellation by pre-determined degrees. Although the rotation process does not change

[1]Note that four time oversampling, i.e., $W = 4$, is enough to represent accurate PAPR [24].

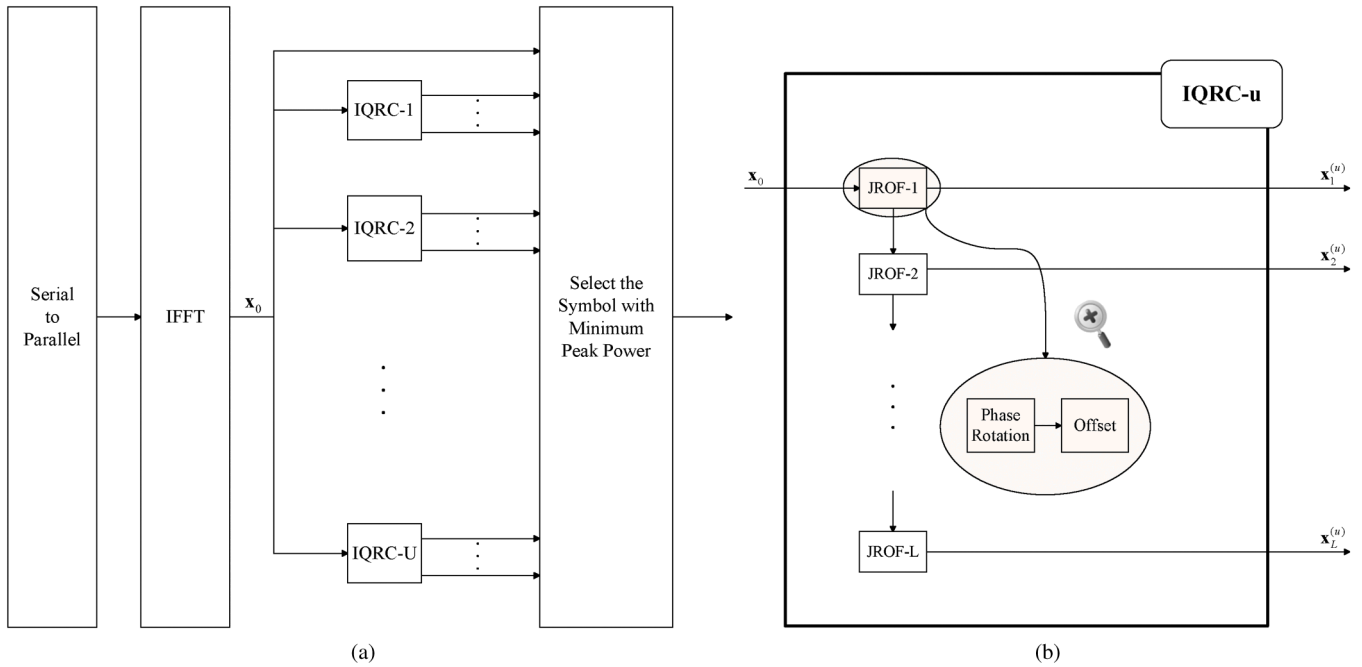

Fig. 1. The transmitter structure of the proposed scheme. (a) The overall structure equipped with U IQRC. (b) The structure of the uth IQRC generating multiple candidate signals $\mathrm{x}_1^{(u)}, \mathrm{x}_2^{(u)}, \cdots, \mathrm{x}_L^{(u)}$.

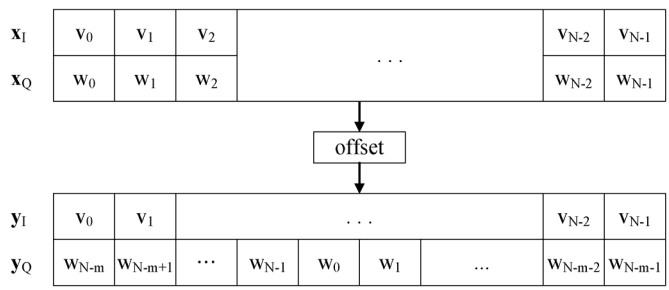

Fig. 2. The process in the offset stage with the offset, m, the in-phase and the quadrature input vectors, $\mathrm{x}_I = [v_0, v_1, \cdots, v_{N-1}]$ and $\mathrm{x}_Q = [w_0, w_1, \cdots, w_{N-1}]$, the in-phase and the quadrature output vectors, $\mathrm{y}_I = [v_0, v_1, \cdots, v_{N-1}]$ and $\mathrm{y}_Q = [w_{N-m}, w_{N-m+1}, \cdots, w_{N-1}, w_0, w_1, \cdots, w_{N-m-2}, w_{N-m-1}]$.

the power of the samples, the in-phase and the quadrature amplitudes may be changed by rotation. For example, a sample $0.1 + j0.9$ becomes $-0.566 + j0.707$ after counter-clockwise rotation of $\frac{\pi}{4}$ degrees, where the amplitude of the quadrature component is decreased. Note that the goal of the phase rotation stage is to suppress the peak amplitude in the incoming samples such that the peak power is reduced eventually.

Although the phase rotation adjusts the amplitude of the in-phase and the quadrature components, it does not change the power of the samples. But if it acts jointly with a cyclic shifting of the components, the peak power can be effectively reduced. Fig. 2 depicts the cyclic shifting stage, where the quadrature component of the output samples from the phase rotation stage is cyclically shifted in time by a certain offset and then combined with the in-phase component in a mis-aligned manner. This operation in fact is similar to that of offset-PSK modulation except the fact that the offset can be a variable. By cyclically shifting the quadrature component, while the in-phase component is intact, this stage aims to achieve a mis-alignment of the in-phase sample with high amplitude and the quadrature sample with high amplitude.

Consider an OFDM symbol, which is the output of the IFFT processor, denoted by x_0. Using x_0 as the input symbol, each IQRC block performs L JROF subblocks in a boot-strapping fashion, where JROF-1 is first executed and then JROF-2 is carried out using the output symbol from the JROF-1, and so on, which is illustrated in Fig. 1(b). The output symbol from JROF-l in IQRC-u is denoted by $\mathrm{x}_l^{(u)} = [x_{l,0}^{(u)}, \cdots, x_{l,N-1}^{(u)}]^{\mathsf{T}}$, for $l = 1, \cdots, L$. In other words, $\mathrm{x}_1^{(u)}$ is the output from JROF-1 for the input x_0, and $\mathrm{x}_2^{(u)}$ is the output from JROF-2 for the input $\mathrm{x}_1^{(u)}$, and so on. In this fashion, $\mathrm{x}_L^{(u)}$ is generated after L different JROF processes one after another.

Let $f_{\theta, m_l^{(u)}}(\cdot)$ denote a function for the JROF-l in IQRC-u, where θ and $m_l^{(u)}$ denote the angle of the phase rotation and the offset of the cyclic shifting, respectively. Assuming that the phases of all the samples in the input symbol are random, or uniformly distributed between 0 and 2π, we consider θ to be a constant value, whereas the offset $m_l^{(u)}$ is variable depending on l and u. Based on these, the output symbol from JROF-l in IQRC-u can be expressed in a recurrence equation as

$$\mathrm{x}_l^{(u)} = f_{\theta, m_l^{(u)}}\left(\mathrm{x}_{l-1}^{(u)}\right), \quad l = 1, \cdots, L, \quad u = 1, \cdots, U \tag{4}$$

where $\mathrm{x}_0^{(u)} = \mathrm{x}_0$ regardless of u. We can rewrite (4) as

$$\mathrm{x}_l^{(u)} = f_{\theta, m_l^{(u)}}^{(l)}(\mathrm{x}_0), \quad l = 1, \cdots, L \tag{5}$$

where

$$f_{\theta, m_l^{(u)}}^{(l)}(\mathrm{x}_0) = \begin{cases} f_{\theta, m_l^{(u)}}\left(\cdots f_{\theta, m_2^{(u)}}\left(f_{\theta, m_1^{(u)}}(\mathrm{x}_0)\right)\right), & 1 \le l \le L, \\ \mathrm{x}_0, & l = 0 \end{cases} \tag{6}$$

is a nested function of $f_{\theta,m_l^{(u)}}(\cdot)$ with a varying offset $m_l^{(u)}$. Since $\mathrm{x}_l^{(u)}$ is a complex vector, it can be written as

$$\mathrm{x}_l^{(u)} = \mathrm{v}_l^{(u)} + j\mathrm{w}_l^{(u)}, \quad l = 0, \cdots, L, \quad u = 1, \cdots, U \tag{7}$$

where $\mathrm{v}_l^{(u)} = [v_{l,0}^{(u)}, \cdots, v_{l,N-1}^{(u)}]^{\mathrm{T}}$ and $\mathrm{w}_l = [w_{l,0}^{(u)}, \cdots, w_{l,N-1}^{(u)}]^{\mathrm{T}}$ represent the in-phase and the quadrature components, respectively. Substituting (7) into (4), we can rewrite (4) as

$$\begin{aligned}\mathrm{x}_l^{(u)} &= f_{\theta,m_l^{(u)}}\left(\mathrm{v}_{l-1}^{(u)} + j\mathrm{w}_{l-1}^{(u)}\right) \\ &= f_{0,m_l^{(u)}}\left(\left(\mathrm{v}_{l-1}^{(u)} + j\mathrm{w}_{l-1}^{(u)}\right)\exp(j\theta)\right) \\ &= \mathrm{v}_{l-1}^{(u)}\cos\theta - \mathrm{w}_{l-1}^{(u)}\sin\theta \\ &\quad + j\mathrm{P}_{m_l^{(u)}}\left(\mathrm{v}_{l-1}^{(u)}\sin\theta + \mathrm{w}_{l-1}^{(u)}\cos\theta\right)\end{aligned} \tag{8}$$

where $\mathrm{P}_{m_l^{(u)}}$ denotes the $N \times N$ circular permutation matrix given by

$$\mathrm{P}_{m_l^{(u)}} = \left[\begin{array}{c|c} \mathrm{O}_{m_l^{(u)},N-m_l^{(u)}} & \mathrm{I}_{m_l^{(u)}} \\ \hline \mathrm{I}_{N-m_l^{(u)}} & \mathrm{O}_{N-m_l^{(u)},m_l^{(u)}} \end{array}\right] \tag{9}$$

where I_m and $\mathrm{O}_{m,n}$ denotes $m \times m$ identity matrix and $m \times n$ zero matrix, respectively. Note that the function $f_{\theta,m_l^{(u)}}(\cdot)$ is a nonlinear process for a complex input vector.

For notational brevity, we rewrite $\mathrm{x}_l^{(u)}$ into a matrix form as

$$\tilde{\mathrm{x}}_l^{(u)} = \begin{bmatrix} \mathrm{v}_l^{(u)} \\ \mathrm{w}_l^{(u)} \end{bmatrix} \tag{10}$$

where $\mathrm{v}_l^{(u)}$ and $\mathrm{w}_l^{(u)}$ are the in-phase and the quadrature components, respectively. We call (10) as a split vector since the real and the imaginary components are separately expressed in one column. The matrix corresponding to the function $f_{\theta,m_l^{(u)}}$ for $\tilde{\mathrm{x}}_l^{(u)}$ is then found as

$$\mathrm{R}_{\theta,m_l^{(u)}} = \left[\begin{array}{c|c} \mathrm{I}\cos\theta & -\mathrm{I}\sin\theta \\ \hline \mathrm{P}_{m_l^{(u)}}\sin\theta & \mathrm{P}_{m_l^{(u)}}\cos\theta \end{array}\right] \tag{11}$$

where I denotes $N \times N$ identity matrix. Although the size of $\mathrm{R}_{\theta,m_l^{(u)}}$ is $2N$, its components are real and nonzero values exist sparsely and regularly in the matrix, which allows a low computational complexity. Then we can rewrite (4) and (5) as

$$\begin{aligned}\tilde{\mathrm{x}}_l^{(u)} &= \mathrm{R}_{\theta,m_l^{(u)}}\tilde{\mathrm{x}}_{l-1}^{(u)} \\ &= \mathrm{G}_l^{(u)}\tilde{\mathrm{x}}_0\end{aligned} \tag{12}$$

where

$$\mathrm{G}_l^{(u)} = \prod_{i=1}^{l}\mathrm{R}_{\theta,m_i^{(u)}}, \quad l = 1, \cdots, L \tag{13}$$

is a matrix for the composite function $f_{\theta,m_l^{(u)}}^{(l)}$.

TABLE I
THE RANDOM SEQUENCE, S, FOR THE OFFSET $m_l^{(u)}$

{75,	209,	122,	32,	30,	233,	101,	179,
145,	32,	240,	137,	32,	162,	27,	113,
243,	67,	124,	253,	50,	75,	131,	112,
249,	229,	36,	48,	20,	117,	13,	234,
10,	153,	69,	230,	216,	173,	224,	239,
191,	195,	100,	84,	183,	39,	42,	34,
26,	47,	114,	111,	75,	34,	57,	76,
3,	234,	86,	187,	41,	193,	241,	29}

Since $\tilde{\mathrm{x}}_l^{(u)}$ is generated from $\tilde{\mathrm{x}}_{l-1}^{(u)}$ in an iterative fashion, $\tilde{\mathrm{x}}_l^{(u)}$ may be statistically correlated with $\tilde{\mathrm{x}}_{l-1}^{(u)}$ in terms of PAPR. If more than one candidates look alike, then those candidates will result in an almost identical PAPR, which degrade the PAPR reduction performance. Thus, the phase rotation and the offset should be carefully selected to obtain improved PAPR reduction performance.

To improve the PAPR reduction performance of the proposed scheme, we pursue two different steps. First, we select the offset $m_l^{(u)}$ from randomly generated sequences. Table I shows the random sequences used in this paper. The offset $m_l^{(u)}$ is expressed as

$$m_l^{(u)} = s_{(u-1)L+l}, \quad l = 1, \cdots, L, \quad u = 1, \cdots, U \tag{14}$$

where s_k is the kth element of S in Table I. Note that randomly generated sequences can be easily implemented by a pseudo random sequence generator based on shift registers. Hence, we assume that both the transmitter and the receiver know upfront these random sequences generated based on an agreed upon seed. Since the effects of an offset on the PAPR reduction performance are hard to theoretically analyzed, we show by numerical simulations that the best offset is a random sequence in Appendix A.

Second, we determine the value of θ as follows:

$$\theta = \frac{\pi}{4}. \tag{15}$$

The proof for (15) is provided in Appendix A. From complexity point of view, this choice of parameters has much advantages. In the next section we analyze the complexity of the proposed scheme in more detail.

B. Proposed Scheme With Reduced Complexity

Consider that computational complexity is quantified by the number of complex multiplications required for the processing. Using (15), we can simplify (8) as

$$\mathrm{x}_l^{(u)} = \frac{1}{\sqrt{2}}\left\{\mathrm{v}_{l-1}^{(u)} - \mathrm{w}_{l-1}^{(u)} + j\mathrm{P}_{m_l^{(u)}}\left(\mathrm{v}_{l-1}^{(u)} + \mathrm{w}_{l-1}^{(u)}\right)\right\} \tag{16}$$

which only requires two real additions in order to find $\mathrm{x}_l^{(u)}$ from $\mathrm{x}_{l-1}^{(u)}$, while (8) requires a complex multiplication by $\exp(j\theta)$. Considering that a scaling factor of $\frac{1}{\sqrt{2}}$ is a constant, we can rewrite (16) as

$$\dot{\mathrm{x}}_l^{(u)} = \dot{\mathrm{v}}_{l-1}^{(u)} - \dot{\mathrm{w}}_{l-1}^{(u)} + j\mathrm{P}_{m_l^{(u)}}\left(\dot{\mathrm{v}}_{l-1}^{(u)} + \dot{\mathrm{w}}_{l-1}^{(u)}\right) \tag{17}$$

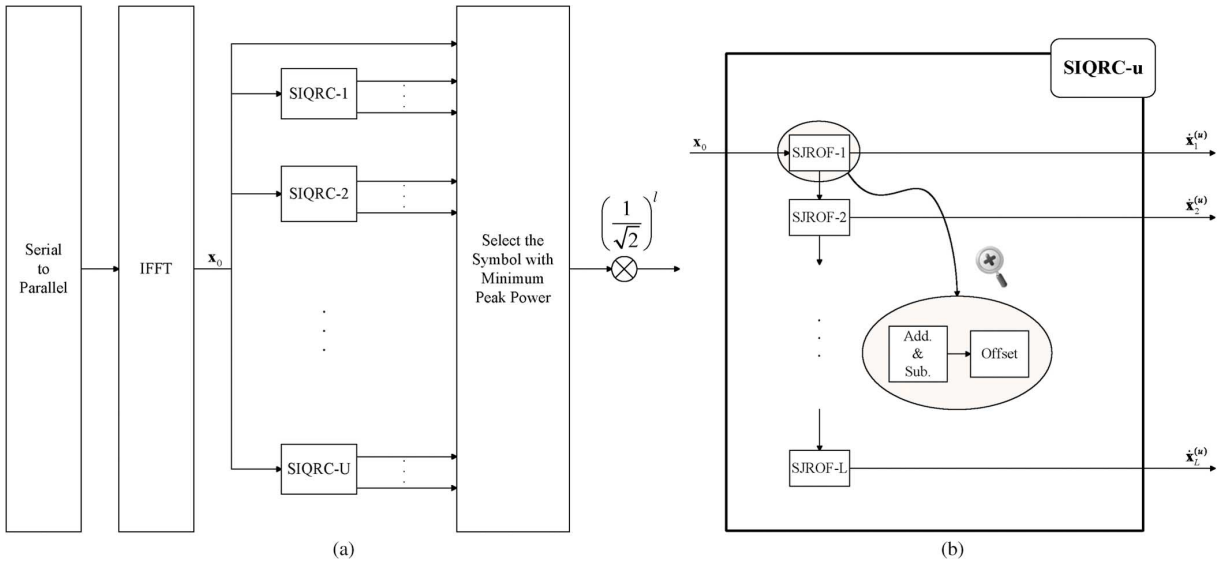

Fig. 3. The transmitter structure of the proposed scheme with reduced complexity. (a) The simplified structure equipped with U SIQRC. (b) The structure of the uth SIQRC generating multiple candidate signals $\dot{\mathrm{x}}_1^{(u)}, \dot{\mathrm{x}}_2^{(u)}, \cdots, \dot{\mathrm{x}}_L^{(u)}$.

where the input vector, $\dot{\mathrm{x}}_{l-1}^{(u)} = \dot{\mathrm{v}}_{l-1}^{(u)} + j\dot{\mathrm{w}}_{l-1}^{(u)}$, and the initial OFDM symbol, $\dot{\mathrm{x}}_0^{(u)} = \mathrm{x}_0^{(u)}$. We can derive that $\dot{\mathrm{x}}_l^{(u)} = \sqrt{2}^l \mathrm{x}_l^{(u)}$ from (16) and (17). Since the power of $\dot{\mathrm{x}}_l^{(u)}$ becomes twice as l increases by 1, the signal with minimum PAPR $\breve{\mathrm{x}}_l^{(u)}$ is selected as following:

$$\breve{\mathrm{x}}_l^{(u)} = \arg\min_{\dot{\mathrm{x}}_l^{(u)}} \quad \frac{1}{2^l} P_l^{(u)} \tag{18}$$

where $P_l^{(u)} = \|\dot{\mathrm{x}}_l^{(u)}\|_\infty^2$. It is clear from (17) that infinity norm computations are required as many as the number of the candidate symbols. The computed results are scaled down by $\frac{1}{2^l}$ since the power of $\dot{\mathrm{x}}_l^{(u)}$ is 2^l times larger than that of $\dot{\mathrm{x}}_0^{(u)}$.

Fig. 3 shows the transmitter structure based on (17) and (18), where the simplified JROF (SJROF) and the simplified IQRC (SIQRC) replace the JROF and the IQRC, respectively, to reduce the complexity. Similarly, the *add. & sub.* block is implemented instead of the phase rotation. The selected candidate symbol, $\dot{\mathrm{x}}_l^{(u)}$, is scaled down by $\left(\frac{1}{\sqrt{2}}\right)^l$ before transmitting to create $\breve{\mathrm{x}}_l^{(u)}$. Thus, it is clear that the scaling is required only once regardless of the number of candidate symbols.

C. Comparison of Computational Complexity

Since the scaling down process is done only once per sample after the symbol with minimum PAPR is determined, the number of such a scaling computation for the proposed transmitter is N in total, which corresponds to $\frac{N}{2}$ complex multiplications. Furthermore, when l is an even number the scaling computation is a division by a power of 2. Since scaling by a power of 2 can be simply implemented by shifting the value in bits, we do not take this into account. Thus, the number of complex multiplications for the scaling computation turns out to be $\frac{N}{4}$.

Table II summarizes the number of complex multiplications to generate candidate symbols for the proposed scheme, the CSPS and the OCSPS methods. In addition, all these schemes require N_s infinity norm computations to find the best symbol with respect to the PAPR. Since the number of real multiplications of one infinity norm is $2N$, we can simply know that the equivalent number of complex multiplications for N_s candidate symbols is $\frac{1}{2}N_sN$. Table III shows an example for the number of complex multiplications including the N_s infinity norm computations when $N = 256$. It is clear that the computational complexity of the proposed scheme is much lower than those of the CSPS and the OCSPS methods.

TABLE II
NUMBER OF COMPLEX MULTIPLICATIONS TO GENERATE MULTIPLE CANDIDATE SYMBOLS OF THE CSPS, OCSPS METHODS, AND THE PROPOSED SCHEME EXCEPT THOSE FOR IFFT OPERATION

Scheme	Main computation	Number of equivalent complex multiplications
CSPS	One N_s-point IFFT and generating N_s candidates	$\frac{N_s}{2}\log_2 N_s + N_sN$ $+(N_s-1)^2N$
OCSPS	Generating N_s candidates	N_sN
Proposed scheme	Scaling operation transmitting the signal	$\frac{N}{4}$

TABLE III
NUMBER OF COMPLEX MULTIPLICATIONS INCLUDING N_s INFINITY NORM COMPUTATIONS WHEN THE NUMBER OF SUBCARRIERS IS 256 AND THE NUMBER OF CANDIDATE SIGNALS IS 16 AND 64 FOR THE CSPS AND OCSPS, RESPECTIVELY, I.E., $N = 256$, $N_s = 16$ FOR CSPS, AND $N_s = 64$ FOR OCSPS

Scheme	Number of equivalent complex multiplication
CSPS	63776
OCSPS	24576
Proposed scheme with $N_s = 16$	2112
Proposed scheme with $N_s = 64$	8256

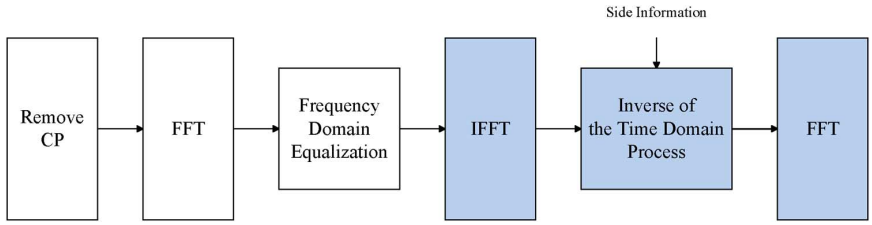

Fig. 4. The receiver structure for the TDSC scheme operated in time domain.

IV. Receiver Structure for the Proposed Scheme

In this section, three simple receiver structures for the proposed scheme are introduced. We first examine the system characteristics of the receiver processing in frequency domain. Then, we derive the ZF and the MMSE estimators for the source symbols. In addition, the ML detector for the source symbols is also derived, since the ML detector blindly decodes the transmitted signal without SI.

A. System Characteristics

The time domain PAPR reduction schemes such as the time domain symbol combining (TDSC) [23] or post-IFFT PAPR reduction schemes [26], [27] have high receiver complexity due to an additional IFFT and FFT pair required at the receiver. Fig. 4 depicts the receiver structure of such schemes. The shaded blocks, which consists of an IFFT and a FFT, are additional costs increasing the complexity. Since the proposed scheme is also a time-domain PAPR reduction scheme, the receiver structure in Fig. 4 can also be used for the proposed scheme. But, instead, the proposed scheme can use a very simple structure, where the shaded blocks can be replaced by only $2(N-1)$ complex multiplications. Details of the simple receiver structure is provided in the following.

Let us denote the channel response and the noise vector in frequency domain by $\mathrm{H} = [H_0, H_1, \cdots, H_{N-1}]^{\mathsf{T}}$ and $\mathrm{n} = [n_0, n_1, \cdots, n_{N-1}]^{\mathsf{T}}$, respectively. We assume that the length of cyclic prefix is long enough to cope with the delay spread of channel. Then the received signal through the multipath fading channel is expressed in frequency domain as

$$\mathrm{Y} = \mathrm{H} \odot \mathrm{D}_N f^{(l)}_{\theta, m_l^{(u)}} \left(\mathrm{D}_N^{-1}\mathrm{X}\right) + \mathrm{n} \tag{19}$$

where $\odot$ denotes element-wise multiplication, and D_N is a DFT matrix given by

$$\mathrm{D}_N = \begin{bmatrix} 1 & 1 & 1 & \cdots & 1 \\ 1 & \mathrm{W}_N & \mathrm{W}_N^2 & \cdots & \mathrm{W}_N^{N-1} \\ 1 & \mathrm{W}_N^2 & \mathrm{W}_N^4 & \cdots & \mathrm{W}_N^{2(N-1)} \\ \vdots & \vdots & \vdots & \ddots & \vdots \\ 1 & \mathrm{W}_N^{N-1} & \mathrm{W}_N^{2(N-1)} & \cdots & \mathrm{W}_N^{(N-1)(N-1)} \end{bmatrix} \tag{20}$$

where $\mathrm{W}_N = e^{-j\frac{2\pi}{N}}$ is a well-known twiddle factor.

Similar to the steps in (5)to (12), the source symbol X is first expressed as a split vector as

$$\tilde{\mathrm{X}} = \begin{bmatrix} \mathrm{Re}(\mathrm{X}) \\ \mathrm{Im}(\mathrm{X}) \end{bmatrix}. \tag{21}$$

Likewise, $\tilde{\mathrm{Y}}$ and $\tilde{\mathrm{n}}$ are defined as $[\mathrm{Re}(\mathrm{Y}^{\mathsf{T}})\ \mathrm{Im}(\mathrm{Y}^{\mathsf{T}})]^{\mathsf{T}}$ and $[\mathrm{Re}(\mathrm{n}^{\mathsf{T}})\ \mathrm{Im}(\mathrm{n}^{\mathsf{T}})]^{\mathsf{T}}$, respectively. In addition, a DFT matrix is rephrased as

$$\tilde{\mathrm{D}}_N = \left[\begin{array}{c|c} \mathrm{Re}(\mathrm{D}_N) & \mathrm{Im}(\mathrm{D}_N) \\ \hline -\mathrm{Im}(\mathrm{D}_N) & \mathrm{Re}(\mathrm{D}_N) \end{array}\right] \tag{22}$$

and an IFFT matrix can also be easily derived as

$$\tilde{\mathrm{D}}_N^{-1} = \frac{1}{N}\tilde{\mathrm{D}}_N^{\mathsf{T}}. \tag{23}$$

Similarly, the channel matrix is expressed as

$$\tilde{\mathrm{H}} = \left[\begin{array}{c|c} \mathrm{Re}\left(diag(\mathrm{H})\right) & -\mathrm{Im}\left(diag(\mathrm{H})\right) \\ \hline \mathrm{Im}\left(diag(\mathrm{H})\right) & \mathrm{Re}\left(diag(\mathrm{H})\right) \end{array}\right]. \tag{24}$$

Then we can rewrite (19) as

$$\begin{aligned} \tilde{\mathrm{Y}} &= \tilde{\mathrm{H}}\tilde{\mathrm{D}}_N \mathrm{G}_l^{(u)} \tilde{\mathrm{D}}_N^{-1}\tilde{\mathrm{X}} + \tilde{\mathrm{n}} \\ &= \tilde{\mathrm{H}}\mathrm{F}_l^{(u)}\tilde{\mathrm{X}} + \tilde{\mathrm{n}} \end{aligned} \tag{25}$$

where

$$\mathrm{F}_l^{(u)} = \frac{1}{N}\tilde{\mathrm{D}}_N \mathrm{G}_l^{(u)} \tilde{\mathrm{D}}_N^{\mathsf{T}}. \tag{26}$$

We can see from (25) that $\mathrm{F}_l^{(u)}$ is a precoding matrix for the input split vector $\tilde{\mathrm{X}}$. It is worth noting that $\mathrm{F}_l^{(u)}$ exhibits some useful properties, which are listed as follows.

Property 1:

(a) $\mathrm{F}_l^{(u)}$ consists of four submatrices and each of them is a sparse matrix called X-matrices. The definition of X-matrix is given in Appendix B.

(b) $\mathrm{F}_l^{(u)}\tilde{\mathrm{X}}$ induce that X_i and X_{N-i} share two subcarriers.

(c) $\mathrm{F}_l^{(u)}$ is an orthogonal matrix, i.e., $\mathrm{F}_l^{(u)^{-1}} = \mathrm{F}_l^{(u)^{\mathsf{T}}}$.

These properties are proved in Appendix B based on some properties of circulant matrices and the orthogonal matrices.

B. Zero-Forcing and MMSE Estimation

If the SI is available at the receiver, a simple estimation for the source symbol can be done by a ZF or an MMSE estimator. Using the property that $\mathrm{F}_l^{(u)}$ is an orthogonal matrix, the ZF solution is derived as

$$\begin{aligned} \hat{\mathrm{X}}_{\mathrm{ZF}} &= \tilde{\mathrm{H}}_{\mathrm{eff}}^{-1}\tilde{\mathrm{Y}} \\ &= \mathrm{F}_l^{(u)^{\mathsf{T}}}\tilde{\mathrm{H}}^{-1}\tilde{\mathrm{Y}} \end{aligned} \tag{27}$$

where $\tilde{\mathrm{H}}_{\mathrm{eff}}$ denotes the effective channel matrix given by $\tilde{\mathrm{H}}_{\mathrm{eff}} = \tilde{\mathrm{H}}\mathrm{F}_l^{(u)}$. The (27) shows that $\hat{\mathrm{X}}_{\mathrm{ZF}}$ is obtained by just multiplying by $\mathrm{F}_l^{(u)^{\mathsf{T}}}$ on the equalized signal $\tilde{\mathrm{H}}^{-1}\tilde{\mathrm{Y}}$. Since each of the four

submatrices of $\mathrm{F}_l^{(u)^{\mathsf{T}}}$ is an X-matrix, multiplying by $\mathrm{F}_l^{(u)^{\mathsf{T}}}$ requires $8(N-1)$ real multiplications which are equivalent to $2(N-1)$ complex multiplications. Thus, the ZF estimator can be implemented with very low complexity.

For the effective channel, the MMSE solution is known as

$$\begin{aligned}\hat{\mathrm{X}}_{\mathrm{MMSE}} &= \left(\tilde{\mathrm{H}}_{\mathrm{eff}}^{\mathsf{T}}\tilde{\mathrm{H}}_{\mathrm{eff}} + \alpha\mathrm{I}\right)^{-1}\tilde{\mathrm{H}}_{\mathrm{eff}}\tilde{\mathrm{Y}} \\ &= \left(\left(\tilde{\mathrm{H}}\mathrm{F}_l^{(u)}\right)^{\mathsf{T}}\left(\tilde{\mathrm{H}}\mathrm{F}_l^{(u)}\right) + \alpha\mathrm{I}\right)^{-1}\left(\tilde{\mathrm{H}}\mathrm{F}_l^{(u)}\right)^{\mathsf{T}}\tilde{\mathrm{Y}} \\ &= \left(\mathrm{F}_l^{(u)^{\mathsf{T}}}\Lambda_H\mathrm{F}_l^{(u)} + \alpha\mathrm{I}\right)^{-1}\mathrm{F}_l^{(u)^{\mathsf{T}}}\tilde{\mathrm{H}}^{\mathsf{T}}\tilde{\mathrm{Y}} \end{aligned} \tag{28}$$

where α is the inverse of SNR and Λ_H denotes $\tilde{\mathrm{H}}^{\mathsf{T}}\tilde{\mathrm{H}} = diag([(|\mathrm{h}|^2)^{\mathsf{T}}(|\mathrm{h}|^2)^{\mathsf{T}}]^{\mathsf{T}})$. Using the matrix inversion lemma, namely $(A+BCD)^{-1} = A^{-1} - A^{-1}B(C^{-1}+DA^{-1}B)^{-1}DA^{-1}$, and the fact that $\mathrm{F}_l^{(u)}$ is an orthogonal matrix, (28) is simplified as

$$\hat{\mathrm{X}}_{\mathrm{MMSE}} = \frac{1}{\alpha}\tilde{\mathrm{F}}_l^{(u)^{\mathsf{T}}}\left(\mathrm{I} - (\alpha\Lambda_H + \mathrm{I})^{-1}\right)\tilde{\mathrm{H}}^{\mathsf{T}}\tilde{\mathrm{Y}} \tag{29}$$

where $(\alpha\Lambda_H + \mathrm{I})$ is a diagonal matrix and $\tilde{\mathrm{H}}^{\mathsf{T}}$ has the same structure as $\tilde{\mathrm{H}}$ in (24). Therefore, $\hat{\mathrm{X}}_{\mathrm{MMSE}}$ can also be computed with very low complexity.

C. Maximal Likelihood Detection

Most of the conventional PAPR reduction schemes assume that SI is sent through the dedicated channel in order to help the receiver decode the transmitted symbols. In practical systems, however, the SI transmission is not an easy or simple task. An SI has to be reliably delivered to the receiver every time an OFDM symbol is transmitted. But the SI can not be included in the regular OFDM symbol, it may be thus necessary to use a dedicated channel for the SI if possible, which sacrifices the overall spectral efficiency. Therefore, it is highly desirable from practical system's point of view to design a PAPR reduction scheme that does not need SI. Motivated by this, we design a receiver that demodulates the transmitted source symbols without SI in the ML fashion.

Let us denote the set of the JROF index as $L = \{0, 1, \cdots, L\}$, the set of the IQRC index as $U = \{1, 2, \cdots, U\}$ and the sequence of split constellations as $C = \{c_0, c_1 \cdots c_{2N-1}\}$, where $c_k + jc_{k+N} \in Q$ for $0 \le k \le N-1$. The split source symbol, $\tilde{\mathrm{X}} \in C$, is mapped from a constellation Q such as M-ary quadrature amplitude modulation (QAM). The ML detection metric for the source symbols is given by

$$\min_{\hat{l}\in\mathrm{L},\hat{u}\in\mathrm{U},\hat{\mathrm{X}}\in\mathrm{C}} \left\|\tilde{\mathrm{Y}} - \tilde{\mathrm{H}}\mathrm{F}_l^{(u)}\tilde{\mathrm{X}}\right\| \tag{30}$$

where $\hat{l}$, $\hat{u}$, and $\hat{\mathrm{X}}$ are l, u, and $\tilde{\mathrm{X}}$ minimizing the ML metric, respectively.

The complexity for computing (30) is very high since the minimization is done for the vector $\tilde{\mathrm{X}}$ with length N. However, if we note the property that $\mathrm{F}_l^{(u)}$ makes X_i and X_{N-i} share two subcarriers, we can simplify (30) as

$$\min_{\hat{l}\in\mathrm{L},\hat{u}\in\mathrm{U}} \sum_{i=0}^{N/2-1} \min_{\hat{\mathrm{X}}_{\Psi_i}\in\mathrm{C}_{\Psi_i}} \left\|\tilde{\mathrm{Y}}_{\Psi_i} - \tilde{\mathrm{H}}_{\Psi_i}\mathrm{F}_{l,\Psi_i}^{(u)}\tilde{\mathrm{X}}_{\Psi_i}\right\| \tag{31}$$

where Ψ_i, for $i = 0, 1, \cdots, \frac{N}{2}-1$, is a set of indices which satisfies the condition that

$$\Psi_i = \begin{cases} \{(k,k)|k = i, N-i, N+i, 2N-i\}, & 1 \le i \le \frac{N}{2}-1 \\ \{(k,k)|k = i, N+i\}, & i = 0 \end{cases} \tag{32}$$

for matrices or

$$\Psi_i = \begin{cases} \{k|k = i, N-i, N+i, 2N-i\}, & 1 \le i \le \frac{N}{2}-1 \\ \{k|k = i, N+i\}, & i = 0 \end{cases} \tag{33}$$

for both vectors and sequences. For $1 \le i \le \frac{N}{2}-1$, $\tilde{\mathrm{Y}}_{\Psi_i}$, $\tilde{\mathrm{X}}_{\Psi_i}$, and C_{Ψ_i} in (31) represent

$$\tilde{\mathrm{Y}}_{\Psi_i} = \begin{bmatrix} \tilde{Y}_{i,i} & \tilde{Y}_{i,N-i} & \tilde{Y}_{i,N+i} & \tilde{Y}_{i,2N-i} \\ \tilde{Y}_{N-i,i} & \tilde{Y}_{N-i,N-i} & \tilde{Y}_{N-i,N+i} & \tilde{Y}_{N-i,2N-i} \\ \tilde{Y}_{N+i,i} & \tilde{Y}_{N+i,N-i} & \tilde{Y}_{N+i,N+i} & \tilde{Y}_{N+i,2N-i} \\ \tilde{Y}_{2N-i,i} & \tilde{Y}_{2N-i,N-i} & \tilde{Y}_{2N-i,N+i} & \tilde{Y}_{2N-i,2N-i} \end{bmatrix} \tag{34a}$$

$$\tilde{\mathrm{X}}_{\Psi_i} = [\,\tilde{X}_i,\, \tilde{X}_{N-i},\, \tilde{X}_{N+i},\, \tilde{X}_{2N-i}\,]^{\mathrm{T}} \tag{34b}$$

and

$$\mathrm{C}_{\Psi_i} = \{c_i, \quad c_{N-i}, \quad c_{N+i}, \quad c_{2N-i}\} \tag{34c}$$

respectively. For $i = 0$, $\tilde{\mathrm{Y}}_{\Psi_i}$, $\tilde{\mathrm{X}}_{\Psi_i}$, and C_{Ψ_i} in (31) represent

$$\tilde{\mathrm{Y}}_{\Psi_i} = \begin{bmatrix} \tilde{Y}_{i,i} & \tilde{Y}_{i,N+i} \\ \tilde{Y}_{N+i,i} & \tilde{Y}_{N+i,N+i} \end{bmatrix} \tag{35a}$$

$$\tilde{\mathrm{X}}_{\Psi_i} = [\,\tilde{X}_i, \quad \tilde{X}_{N+i}\,]^{\mathrm{T}} \tag{35b}$$

and

$$\mathrm{C}_{\Psi_i} = \{c_i, \quad c_{N+i}\} \tag{35c}$$

respectively. Fig. 5 shows the ML detector structure. We can find the SI, $\hat{l}$ and $\hat{u}$, and the best $\hat{\mathrm{X}}$ satisfying (31).

If SI is given at the receiver, i.e., both l and u are known, we minimize the ML metric with respect to only $\tilde{\mathrm{X}}_{\Psi_i}$. Thus, (31) can be further simplified as

$$\min_{\tilde{\mathrm{X}}_{\Psi_i}\in\mathrm{C}_{\Psi_i}} \left\|\tilde{\mathrm{Y}}_{\Psi_i} - \tilde{\mathrm{H}}_{\Psi_i}\mathrm{F}_{l,\Psi_i}^{(u)}\tilde{\mathrm{X}}_{\Psi_i}\right\|, \quad 0 \le i \le \frac{N}{2}-1. \tag{36}$$

By well-known near-ML detection methods such as the sphere decoding, the computational complexity for solving (31) and (36) can be reduced, although the specific algorithm of the sphere decoding is out of the scope of this paper.

V. Simulation Results

This section presents the simulation results including the complementary cumulative distribution function (CCDF) of the PAPR and the BER of the proposed scheme. We assume that the number of subcarriers is 256, i.e., $N = 256$, and both

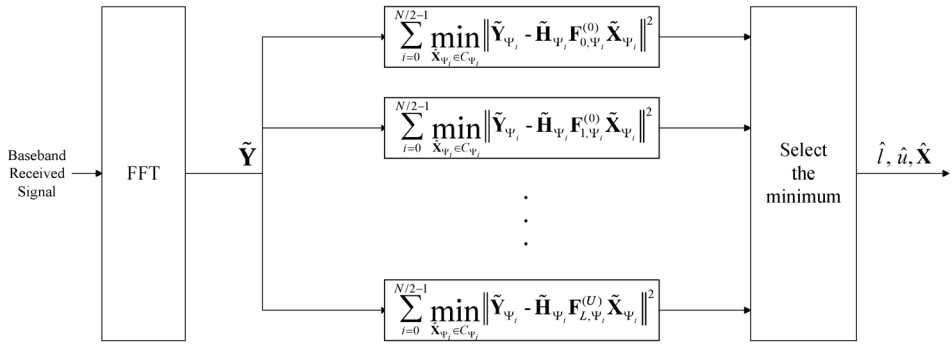

Fig. 5. The proposed ML detector for the transmitted source symbol.

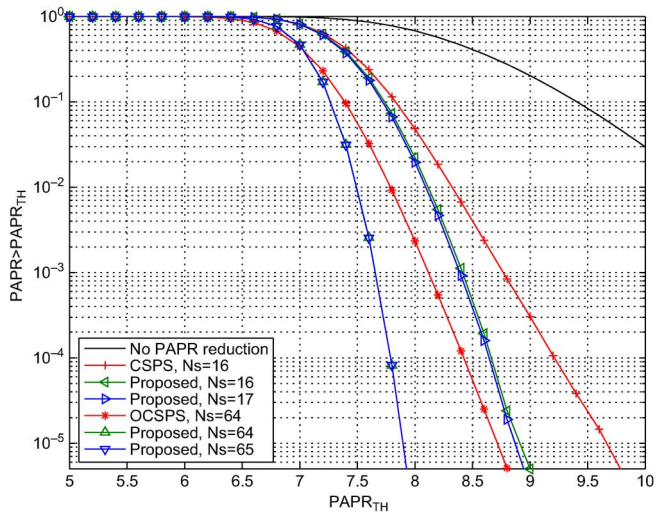

Fig. 6. Performance comparisons among no PAPR reduction, the CSPS method, the OCSPS method, and the proposed schemes with $N_s = 17$, $N_s = 65$, $N_s = 16$ and $N_s = 64$ in terms of the CCDF of PAPR when $N = 256$, the oversampling factor, $W = 4$, and QPSK mapping are used.

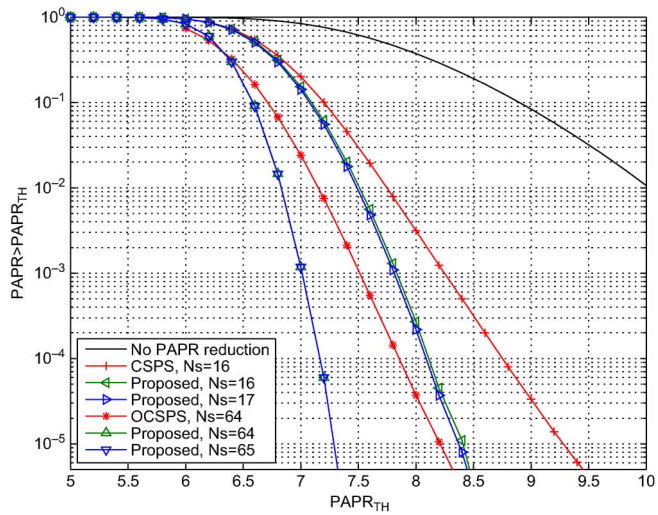

Fig. 7. Performance comparisons among no PAPR reduction, the CSPS method, the OCSPS method, and the proposed schemes with $N_s = 17$, $N_s = 65$, $N_s = 16$, and $N_s = 64$ in terms of the CCDF of the PAPR when the IFFT size $N = 256$, the oversampling factor $W = 1$, and QPSK mapping are used.

the quadrature phase shift keying (QPSK) and the 16-QAM are used for the OFDM symbols.

A. PAPR Reduction Performance

The PAPR reduction performance is commonly measured by CCDF for the PAPR reduction schemes. The CCDF presents the probability that the PAPR of an OFDM symbol is larger than a given threshold value, which is expressed as

$$\text{Prob}[\text{PAPR} > \text{PAPR}_{\text{TH}}]. \tag{37}$$

The PAPR reduction performance of our proposed scheme is compared with the CSPS and the OCSPS methods since they also aim at low complexity and high PAPR reduction performance. The simulation results are presented in Fig. 6. We consider the cases that the number of candidate symbols are 16 and 64 for the CSPS and the OCSPS methods, respectively, which are the most superior cases in terms of the CCDF of the PAPR as presented in [22]. Since the proposed scheme generates $L \times U + 1$ candidates, we consider the cases of ($U = 2$, $L = 8$), and ($U = 8$, $L = 8$), which make 17 and 65 candidate symbols, respectively. Note that the offset $m_l^{(u)}$ is tabulated as a function of u in Table I.

Fig. 6 compares the CCDF of the PAPR of the proposed scheme when $N_s = 17$ and $N_s = 65$ against those of the CSPS and the OCSPS methods when the oversampling factor is 4, i.e., $W = 4$. The proposed scheme with $N_s = 17$ and $N = 65$ outperforms the CSPS and the OCSPS methods by far. For a fair comparison with the CSPS and the OCSPS methods, we also plotted the proposed scheme with $N_s = 16$ and $N_s = 64$ (see dotted lines). In those cases, the original OFDM symbol x_0 is excluded from the candidates. Interestingly, the performance results show that excluding the original OFDM symbol rarely affects the performance. In other words, the proposed schemes with $N_s = 16$ and $N_s = 64$ still overwhelm the conventional methods. In Fig. 7, the CCDFs of the PAPRs are depicted when the oversampling factor is 1, i.e., $W = 1$. This shows the same order of curves as those in Fig. 6.

B. System Information Detection and BER Performance

The proposed ML detector needs to detect SIs accurately, which otherwise can not decode the transmitted OFDM symbols. Thus, it is important to examine the rate of correct detection of SI. Assume that the systems undergo Rayleigh multipath fading channel with 10 channel taps, each of which is complex Gaussian distributed, and the channel has unit power in total. We

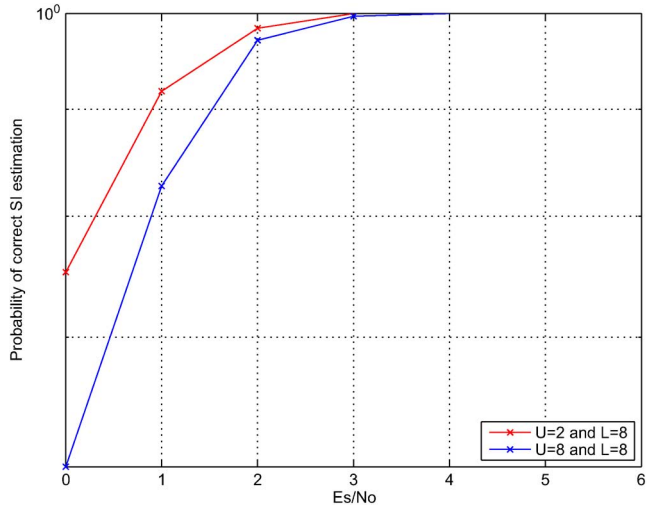

Fig. 8. Probability that SI is correctly decided among the proposed schemes with $(U = 2, L = 8)$, and $(U = 8, L = 8)$ over the Rayleigh 10-tap frequency selective channel when the IFFT size, $N = 256$, and QPSK mapping are used versus average SNR [dB].

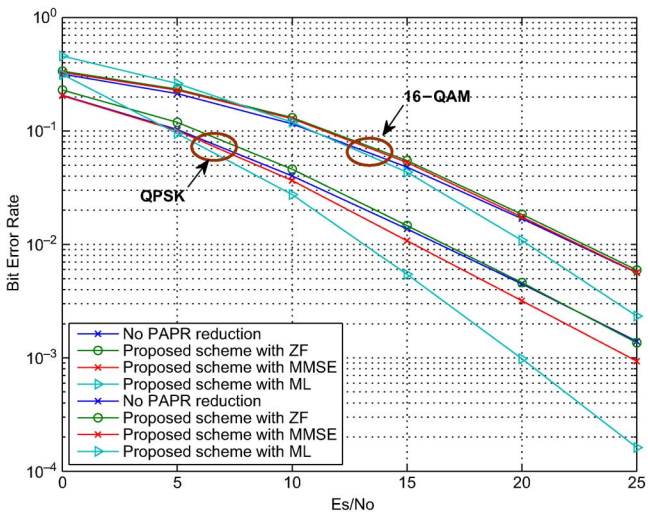

Fig. 9. Bit error rate performances of the unprocessed OFDM transmission and the proposed scheme for the ML detector, the hard decisions with the MMSE and the ZF estimators with $N_s = 65$ over the Rayleigh 10-tap frequency selective channel when the IFFT size, $N = 256$ versus average SNR [dB]. Both the QSPK and the 16-QAM are used.

also assume that cyclic prefix is larger than the channel length (delay spread) and the channel state information (CSI) is fully available at the receiver. Fig. 8 shows that the proposed scheme detects SIs by the ML metric in (31) with high accuracy when the average SNR is higher than 4 dB.

Based on the assumptions on the channel, BER performances are evaluated for various receiver structures when both the QPSK and the 16-QAM are used as a subcarrier modulation. Fig. 9 plots the BER performances for these various receivers. For comparisons, the BER performance of the OFDM system with no PAPR reduction is also plotted where ZF equalization is assumed. The BER performances of the ZF and the MMSE estimator with hard decision are nearly the same as that of OFDM systems with no PAPR reduction scheme for the 16-QAM, but the MMSE estimator for the QPSK shows 1.0 dB -1.5 dB superior BER performance to the no PAPR reduction scheme. The ML detector outperforms by far both the ZF and the MMSE estimators with hard decision.

The reason why the ML detector outperforms the other estimators is that two source samples in the original OFDM symbol share two subcarriers. In other words, two samples are loaded to the corresponding two subcarriers, which mitigates the adverse effect of the frequency selectivity. In both CSPS and OCSPS schemes, the PAPR reduction processes do not affect the BER performances since they are based on PTS scheme. Thus, we do not consider BERs of both CSPS and OCSPS schemes.

Since the purpose of the PAPR reduction is to avoid the signal distortion after the signal is passed through HPA, in this paper, we consider the nonlinear effects of HPA on the BER performance of our proposed scheme. As a HPA model, we use the Rapp's formula for the solid state power amplifier (SSPA) that is given as [28]

$$r_{out} = \frac{r_{in}}{\left(1 + \left(\frac{r_{in}}{V_{sat}}\right)^{2p}\right)^{\frac{1}{2p}}} \tag{38}$$

where r_{in}, r_{out}, V_{sat}, and p are the input amplitude, the output amplitude, the saturating amplitude, and an integer, respectively. The nonlinear distortion is characterized by the input back-off (IBO) defined as

$$\text{IBO} \triangleq 10 \log_{10} \frac{V_{sat}^2}{\langle P_{In} \rangle} \tag{39}$$

where P_{In} denotes the average input power.

The simulated BER performances when HPA is used at the transmitter are shown in Fig. 10. We consider the both the Rayleigh and the AWGN channel. In both the channels, the BER performances of the proposed scheme are much less degraded than the OFDM transmission with no PAPR reduction, since the lowered peak power prevents significant signal distortion.

VI. Conclusion

This paper proposes a novel PAPR reduction scheme with low complexity at the transmitter. The proposed scheme requires only a single IFFT processor at the transmitter since the candidate symbol generation and selection process are all done in time-domain. In addition, it requires less computational complexity than the conventional methods. More importantly, the proposed scheme offers far superior performance to the conventional methods, such as CSPS and OCSPS, in terms of the CCDF of the PAPR.

The ML detector for the transmitted source symbols, which do not require the SI at the receiver, were derived. The simple ZF and the MMSE estimators for the transmitted source symbols, which are available when the SI is given at the receiver, were also derived. The ML detector shows the better performance than the hard decisions with ZF, MMSE estimators and the unprocessed OFDM symbol in terms of BER. The hard decisions with the ZF estimator shows nearly the same performance as the case of the unprocessed OFDM transmission and the hard decision with MMSE estimator shows 1.0–1.5 dB superior performance to the ZF case.

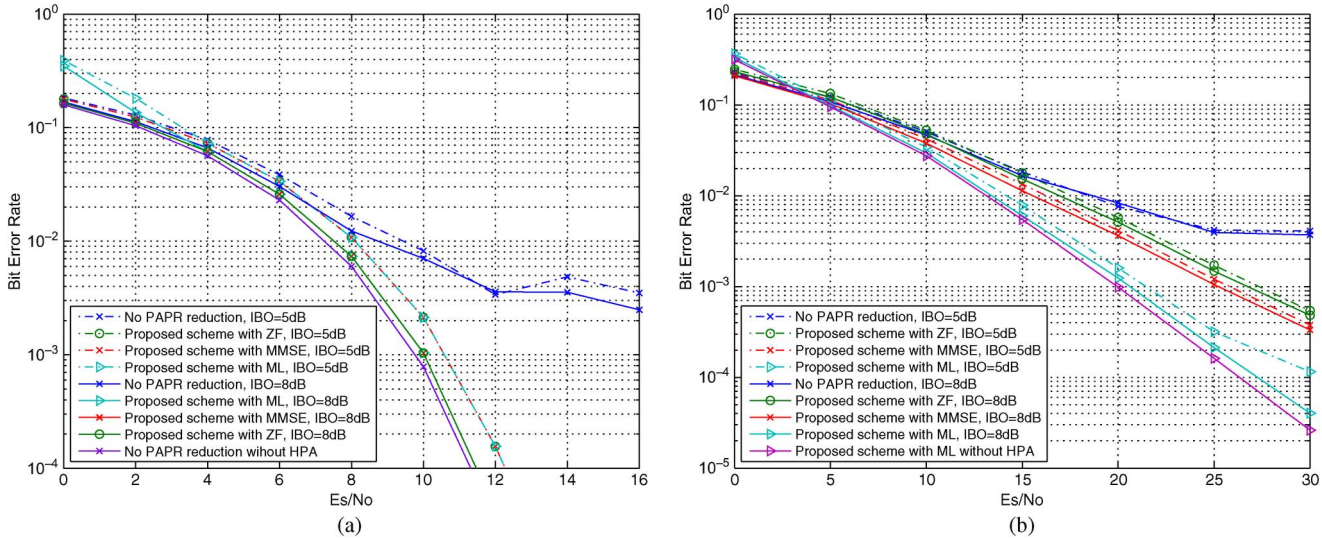

Fig. 10. Bit error rate performance of the proposed scheme over (a) AWGN channel and (b) Rayleigh 10-tap frequency selective channel when SSPA with IBO $=$ 5 dB (or 8 dB) and $p = 2$ is equipped in the transmitter.

APPENDIX A

Equation (15) is proved as follows. For the notation brevity, we use m_l instead of $m_l^{(u)}$ and abbreviate $\cos\theta$ and $\sin\theta$ as c and s, respectively. Suppose an OFDM symbol, which is the output of the IFFT processor, is written as $\mathrm{x}_0 = [x_{0,0}, x_{0,1}, \cdots, x_{0,N-1}]^{\mathsf{T}}$. Using (8), the candidate symbol from the first JROF is given as

$$x_{1,n} = v_{0,n}\boldsymbol{c} - w_{0,n}\boldsymbol{s} + j(v_{0,n+m_1}\boldsymbol{s} + w_{0,n+m_1}\boldsymbol{c}) \quad (40)$$

where n is the sample index ($0 \le n \le N-1$) and m_1 is the sample offset in the quadrature component for the first JROF. Taking this as the input, the candidate symbol from the second JROF is obtained as

$$\begin{aligned} x_{2,n} &= v_{1,n}\boldsymbol{c} - w_{1,n}\boldsymbol{s} + j(v_{1,n+m_2}\boldsymbol{s} + w_{1,n+m_2}\boldsymbol{c}) \\ &= (v_{0,n}\boldsymbol{c} - w_{0,n}\boldsymbol{s})\boldsymbol{c} - (v_{0,n+m_1}\boldsymbol{s} + w_{0,n+m_1}\boldsymbol{c})\boldsymbol{s} \\ &\quad + j(v_{0,n+m_2}\boldsymbol{c} - w_{0,n+m_2}\boldsymbol{s})\boldsymbol{s} \\ &\quad + j(v_{0,n+m_1+m_2}\boldsymbol{s} + w_{0,n+m_1+m_2}\boldsymbol{c})\boldsymbol{c} \end{aligned} \quad (41)$$

where m_2 is the quadrature sample offset in the second JROF. Similarly, the output from the third JROF is written as

$$\begin{aligned} x_{3,n} &= v_{2,n}\boldsymbol{c} - w_{2,n}\boldsymbol{s} + j(v_{2,n+m_3}\boldsymbol{s} + w_{2,n+m_3}\boldsymbol{c}) \\ &= \{(v_{0,n}\boldsymbol{c} - w_{0,n}\boldsymbol{s})\boldsymbol{c} - (v_{0,n+m_1}\boldsymbol{s} + w_{0,n+m_1}\boldsymbol{c})\boldsymbol{s}\}\,\boldsymbol{c} \\ &\quad - \{(v_{0,n+m_2}\boldsymbol{c} - w_{0,n+m_2}\boldsymbol{s})\boldsymbol{s} \\ &\qquad + (v_{0,n+m_1+m_2}\boldsymbol{s} + w_{0,n+m_1+m_2}\boldsymbol{c})\boldsymbol{c}\}\,\boldsymbol{s} \\ &\quad + j\{(v_{0,n+m_3}\boldsymbol{c} - w_{0,n+m_3}\boldsymbol{s})\boldsymbol{c} \\ &\qquad - (v_{0,n+m_1+m_3}\boldsymbol{s} + w_{0,n+m_1+m_3}\boldsymbol{c})\boldsymbol{s}\}\,\boldsymbol{s} \\ &\quad + j\{(v_{0,n+m_2+m_3}\boldsymbol{c} - w_{0,n+m_2+m_3}\boldsymbol{s})\boldsymbol{s} \\ &\qquad + (v_{0,n+m_1+m_2+m_3}\boldsymbol{s} + w_{0,n+m_1+m_2+m_3}\boldsymbol{c})\boldsymbol{c}\}\boldsymbol{c}. \end{aligned} \quad (42)$$

In the same manner, the candidate symbol from the lth JROF can be generalized as

$$\begin{aligned} x_{l,n} = &\sum_{i\in\Omega_{l-1}} (\alpha_i v_{0,n+i} + \beta_i w_{0,n+i}) \\ &+ j\sum_{i\in\Omega_l - \Omega_{l-1}} (\gamma_i v_{0,n+i} + \delta_i w_{0,n+i}) \end{aligned} \quad (43)$$

where Ω_l is a set of sample indices and consists of a sum of all possible combinations of the elements in $\{0, m_1, m_2, \cdots, m_l\}$; the weighting factors α_i, β_i, γ_i, and δ_i are products of l sinusoidal functions. For example, in the case of $l = 3$, $\Omega_3 = \{0, m_1, m_2, m_3, m_1+m_2, m_1+m_3, m_2+m_3, m_1+m_2+m_3\}$ and $\Omega_2 = \{0, m_1, m_2, m_1+m_2\}$, which results in $\Omega_3 - \Omega_2 = \{m_3, m_1+m_3, m_2+m_3, m_1+m_2+m_3\}$. Thus, we can rewrite (42) as

$$\begin{aligned} x_{l,n} = &\sum_{i\in\Omega_2} (\alpha_i v_{0,n+i} + \beta_i w_{0,n+i}) \\ &+ j\sum_{i\in\Omega_3 - \Omega_2} (\gamma_i v_{0,n+i} + \delta_i w_{0,n+i}) \end{aligned} \quad (44)$$

where $\alpha_0 = ccc$, $\alpha_{m_1} = ssc$, $\alpha_{m_2} = css$, and $\alpha_{m_1+m_2} = scs$. We can also easily find β_i, γ_i, and δ_i by the same manner.

Given the fact that the samples in an output OFDM symbol exhibit Gaussian-like distribution, we can regard $x_{l,n}$ as a weighted sum of Gaussian random variables. In order that $x_{l,n}$ is generated from all of $v_{0,i}$ and $w_{0,i}$ for $i \in \Omega_l$ with the same weighting factors, the absolute values of them should be the same. For this condition, θ should satisfy the equation $|\cos\theta| = |\sin\theta|$ where the solutions are $\theta = \pm\frac{\pi}{4} \pm \frac{\pi}{2}$. Without loss of generality, we choose $\theta = \frac{\pi}{4}$.

In order to show that a random sequence improves the PAPR reduction performance of the proposed scheme, we consider three different types of phase rotations and offsets. For the phase

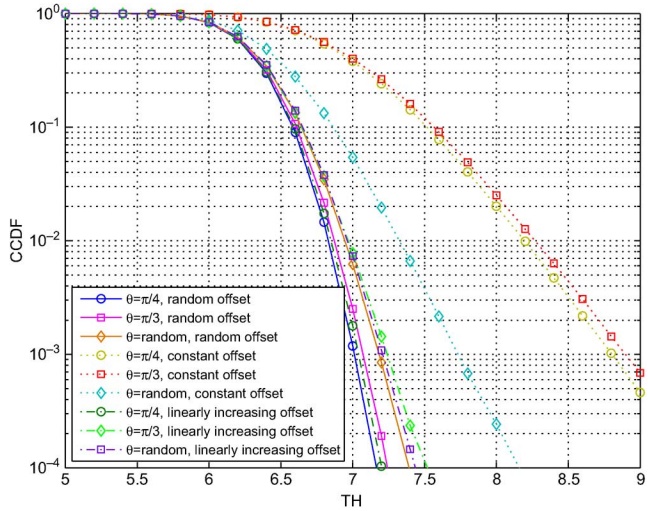

Fig. 11. Performance comparisons among the various phase rotation and the offset with $U = 8$, $L = 8$ in terms of the CCDF of the PAPR when the IFFT size $N = 256$, the oversampling factor $W = 1$, and QPSK mapping are used.

rotation, $\frac{\pi}{3}$ and random phases are considered as well as $\frac{\pi}{4}$. For the offset, constant offset and linearly increasing offset are considered as well as the random offset. The offset $m_l^{(u)}$ is expressed as

$$m_l^{(u)} = 1, \quad l = 1, \cdots, L, \quad u = 1, \cdots, U \tag{45}$$

for the constant offset

$$m_l^{(u)} = (u-1)L + l, \quad l = 1, \cdots, L, \quad u = 1, \cdots, U \tag{46}$$

for the linearly increasing offset.

Fig. 11 shows the simulation results, where the phase rotation of $\frac{\pi}{4}$ and the random offset work together to provide the best performance.

Appendix B
Definition of the X-Matrix

Definition 1: Let A be an $m \times m$ square matrix where m is an even number. A is an X-matrix if it follows

(a) For the kth column, the nonzeros values are located only at the kth row and $N-k$th row, for $1 \le k \le N-1$.

(b) Only (1,1) component of A can be a nonzero value at the first row and the first column.

The X-matrix, denoted as X, is given at the bottom of the page, where $\chi_{i,j}$ is (i,j) entry of X. Since the nonzeros values are on the shape of alphabet X, we name these forms of matrices X-matrix.

We can easily find by basic matrix calculations that X-matrices follow the lemma.

Lemma 1: Let A and B be $m \times m$ X-matrices.

(a) A^{H} is an X-matrix, if A is an X-matrix;

(b) $\mathrm{A} + \mathrm{B}$ is an X-matrix;

(c) AB is an X-matrix.

Appendix C
Proof of Property

Proof: $\mathrm{F}_l^{(u)}$ consists of four submatrices and each of them is a sparse matrix called X-matrices.

As shown in (11), $\mathrm{R}_{\theta,m_l^{(u)}}$ consists of four submatrices and all of them are circulant matrices. Some properties of circulant matrices are given in *Theorem 1* and 2 [29].

Theorem 1: Let A and B be $m \times m$ circulant matrices.

(a) for any scalar α and β, $\alpha\mathrm{A} + \beta\mathrm{B}$ is circulant;

(b) for any positive integer r, A^r is circulant,

(c) A^{-1} is circulant, if A is circulant;

(d) AB is circulant.

Theorem 2: Let A be the $m \times m$ circulant matrices $\mathrm{circ}(a_1, \cdots, a_m)$. Then

$$\mathrm{A} = \frac{1}{m}\mathrm{D}_m \Lambda \mathrm{D}_m^{\mathrm{H}} \tag{47}$$

where $\Lambda = diag(\delta_1, \cdots, \delta_m)$, $\delta_k = a_1 + a_2\lambda_k^1 + \cdots + a_m\lambda_k^{m-1}$, and $\lambda_1, \cdots, \lambda_m$ are the m solutions to the polynomial equation $\lambda^m - 1$; that is, $\lambda_k = \theta^{k-1}$, where $\theta = \exp(\frac{2\pi j}{m})$.

It can be easily shown that the four submatrices of $\mathrm{G}_l^{(u)}$ are circulant by the definition of $\mathrm{G}_l^{(u)}$ in (13) and *Theorem 1*. If we apply *Theorem 2* to each submatrix of $\mathrm{G}_l^{(u)}$, it can be rewritten as

$$\mathrm{G}_l^{(u)} = \frac{1}{N}\left[\begin{array}{c|c} \mathrm{D}_N\Lambda_{l1}^{(u)}\mathrm{D}_N^{\mathrm{H}} & \mathrm{D}_N\Lambda_{l2}^{(u)}\mathrm{D}_N^{\mathrm{H}} \\ \hline \mathrm{D}_N\Lambda_{l3}^{(u)}\mathrm{D}_N^{\mathrm{H}} & \mathrm{D}_N\Lambda_{l4}^{(u)}\mathrm{D}_N^{\mathrm{H}} \end{array}\right] \tag{48}$$

$$\mathrm{X} = \begin{bmatrix} \chi_{0,0} & 0 & \cdots & \cdots & \cdots & \cdots & \cdots & 0 \\ 0 & \chi_{1,1} & 0 & \cdots & \cdots & \cdots & 0 & \chi_{1,N-1} \\ \vdots & 0 & \chi_{,22} & 0 & \cdots & 0 & \chi_{2,N-2} & 0 \\ \vdots & \vdots & 0 & \ddots & \vdots & \iddots & 0 & \vdots \\ \vdots & \vdots & \vdots & \cdots & \chi_{N/2,N/2} & \cdots & \vdots & \vdots \\ \vdots & \vdots & 0 & \iddots & \vdots & \ddots & 0 & \vdots \\ \vdots & 0 & \chi_{N-2,2} & 0 & \cdots & 0 & \chi_{N-2,N-2} & 0 \\ 0 & \chi_{N-1,1} & 0 & \cdots & \cdots & \cdots & 0 & \chi_{N-1,N-1} \end{bmatrix}$$

where $\Lambda_{l1}^{(u)}$, $\Lambda_{l2}^{(u)}$, $\Lambda_{l3}^{(u)}$, and $\Lambda_{l4}^{(u)}$ are eigenvalue matrices of the four submatrices of $G_l^{(u)}$, respectively. Substituting (22) and (48) into (26), $\mathrm{F}_l^{(u)}$ can be found as

$$\mathrm{F}_l^{(u)} = \frac{1}{N^2}\left[\begin{array}{c|c} \Phi_{l,1}^{(u)} & \Phi_{l,2}^{(u)} \\ \hline \Phi_{l,3}^{(u)} & \Phi_{l,4}^{(u)} \end{array}\right] \tag{49}$$

where

$$\begin{aligned}
\Phi_{l,1}^{(u)} =& \mathrm{Re}(\mathrm{D}_N)\mathrm{D}_N\Lambda_{l1}^{(u)}\mathrm{D}_N^{\mathrm{H}}\mathrm{Re}(\mathrm{D}_N) \\
&+ \mathrm{Im}(\mathrm{D}_N)\mathrm{D}_N\Lambda_{l2}^{(u)}\mathrm{D}_N^{\mathrm{H}}\mathrm{Re}(\mathrm{D}_N) \\
&+ \mathrm{Re}(\mathrm{D}_N)\mathrm{D}_N\Lambda_{l3}^{(u)}\mathrm{D}_N^{\mathrm{H}}\mathrm{Im}(\mathrm{D}_N) \\
&+ \mathrm{Im}(\mathrm{D}_N)\mathrm{D}_N\Lambda_{l4}^{(u)}\mathrm{D}_N^{\mathrm{H}}\mathrm{Im}(\mathrm{D}_N) \qquad (50a) \\
\Phi_{l,2}^{(u)} =& -\mathrm{Re}(\mathrm{D}_N)\mathrm{D}_N\Lambda_{l1}^{(u)}\mathrm{D}_N^{\mathrm{H}}\mathrm{Im}(\mathrm{D}_N) \\
&- \mathrm{Im}(\mathrm{D}_N)\mathrm{D}_N\Lambda_{l2}^{(u)}\mathrm{D}_N^{\mathrm{H}}\mathrm{Im}(\mathrm{D}_N) \\
&+ \mathrm{Re}(\mathrm{D}_N)\mathrm{D}_N\Lambda_{l3}^{(u)}\mathrm{D}_N^{\mathrm{H}}\mathrm{Re}(\mathrm{D}_N) \\
&+ \mathrm{Im}(\mathrm{D}_N)\mathrm{D}_N\Lambda_{l4}^{(u)}\mathrm{D}_N^{\mathrm{H}}\mathrm{Re}(\mathrm{D}_N) \qquad (50b) \\
\Phi_{l,3}^{(u)} =& -\mathrm{Im}(\mathrm{D}_N)\mathrm{D}_N\Lambda_{l1}^{(u)}\mathrm{D}_N^{\mathrm{H}}\mathrm{Re}(\mathrm{D}_N) \\
&+ \mathrm{Re}(\mathrm{D}_N)\mathrm{D}_N\Lambda_{l2}^{(u)}\mathrm{D}_N^{\mathrm{H}}\mathrm{Re}(\mathrm{D}_N) \\
&- \mathrm{Im}(\mathrm{D}_N)\mathrm{D}_N\Lambda_{l3}^{(u)}\mathrm{D}_N^{\mathrm{H}}\mathrm{Im}(\mathrm{D}_N) \\
&+ \mathrm{Re}(\mathrm{D}_N)\mathrm{D}_N\Lambda_{l4}^{(u)}\mathrm{D}_N^{\mathrm{H}}\mathrm{Im}(\mathrm{D}_N) \qquad (50c) \\
\Phi_{l,4}^{(u)} =& -\mathrm{Im}(\mathrm{D}_N)\mathrm{D}_N\Lambda_{l1}^{(u)}\mathrm{D}_N^{\mathrm{H}}\mathrm{Im}(\mathrm{D}_N) \\
&- \mathrm{Re}(\mathrm{D}_N)\mathrm{D}_N\Lambda_{l2}^{(u)}\mathrm{D}_N^{\mathrm{H}}\mathrm{Im}(\mathrm{D}_N) \\
&- \mathrm{Im}(\mathrm{D}_N)\mathrm{D}_N\Lambda_{l3}^{(u)}\mathrm{D}_N^{\mathrm{H}}\mathrm{Re}(\mathrm{D}_N) \\
&+ \mathrm{Re}(\mathrm{D}_N)\mathrm{D}_N\Lambda_{l4}^{(u)}\mathrm{D}_N^{\mathrm{H}}\mathrm{Re}(\mathrm{D}_N). \qquad (50d)
\end{aligned}$$

On the other hand, the columns of $\mathrm{Re}(\mathrm{D}_N)$ and $\mathrm{Im}(\mathrm{D}_N)$ in (50) are discrete cosine and sine waveforms respectively, which can be expressed as

$$\begin{aligned}
\mathrm{Re}(\mathrm{D}_N) &= \left[\cos\left(\frac{2\pi}{N}0\cdot\tau\right)\cdots\cos\left(\frac{2\pi}{N}(N-1)\cdot\tau\right)\right], \\
\mathrm{Im}(\mathrm{D}_N) &= \left[\sin\left(\frac{2\pi}{N}0\cdot\tau\right)\cdots\sin\left(\frac{2\pi}{N}(N-1)\cdot\tau\right)\right] \qquad (51)
\end{aligned}$$

where $\tau = [0\ 1\ \cdots\ N-1]^{\mathsf{T}}$. The kth column of $\mathrm{D}_N^{\mathrm{H}}\mathrm{Re}(\mathrm{D}_N)$ in (50), $\mathrm{D}_N^{\mathrm{H}}\cos(\frac{2\pi}{N}k\cdot\tau)$, is the IFFT result of $\cos(\frac{2\pi}{N}k\cdot\tau)$, where only both kth and $(N-k)$th entries of $\mathrm{D}_N^{\mathrm{H}}\cos(\frac{2\pi}{N}k\cdot\tau)$ have nonzero values. The same result can be found on $\mathrm{D}_N^{\mathrm{H}}\sin((2\pi/N)k\cdot\tau)$. This is a well-known result in that the inverse Fourier transform of a sinusoidal waveform produces two impulses at the symmetrical frequency positions. Therefore, we can conclude that both $\mathrm{D}_N^{\mathrm{H}}\mathrm{Re}(\mathrm{D}_N)$ and $\mathrm{D}_N^{\mathrm{H}}\mathrm{Im}(\mathrm{D}_N)$ are X-matrices. We can also induce based on the *Lemma 1*-(a) that both $\mathrm{Re}(\mathrm{D}_N)\mathrm{D}_N$ and $\mathrm{Im}(\mathrm{D}_N)\mathrm{D}_N$ are X-matrices, since they are Hermitians of $\mathrm{D}_N^{\mathrm{H}}\mathrm{Re}(\mathrm{D}_N)$ and $\mathrm{D}_N^{\mathrm{H}}\mathrm{Im}(\mathrm{D}_N)$, respectively. Since $\Phi_{l,\kappa}^{(u)}$, $\kappa = 1,\cdots,4$ in (50) are sum of sequential multiplication of X-matrices, it is induced that $\Phi_{l,\kappa}^{(u)}$ is also an X-matrix from the *Lemma 1*. Therefore, the four submatrices of $\mathrm{F}_l^{(u)}$ are X-matrices. ■

Proof: $\mathrm{F}_l^{(u)}\tilde{\mathrm{X}}$ induce that X_i and X_{N-i} share two subcarriers.

Let $\tilde{\mathrm{Z}} = [\tilde{Z}_0, \tilde{Z}_1, \cdots, \tilde{Z}_{2N-1}]^{\mathsf{T}}$ be $\mathrm{F}_l^{(u)}\tilde{\mathrm{X}}$. Then $\tilde{\mathrm{Z}}$ can be expressed as

$$\begin{aligned}
\tilde{\mathrm{Z}} &= \mathrm{F}_l^{(u)}\tilde{\mathrm{X}} \\
&= \frac{1}{N^2}\left[\begin{array}{c|c} \Phi_{l,1}^{(u)} & \Phi_{l,2}^{(u)} \\ \hline \Phi_{l,3}^{(u)} & \Phi_{l,4}^{(u)} \end{array}\right]\left[\frac{\mathrm{Re}(\mathrm{X})}{\mathrm{Im}(\mathrm{X})}\right] \\
&= \frac{1}{N^2}\left[\frac{\Phi_{l,1}^{(u)}\mathrm{Re}(\mathrm{X}) + \Phi_{l,2}^{(u)}\mathrm{Im}(\mathrm{X})}{\Phi_{l,3}^{(u)}\mathrm{Re}(\mathrm{X}) + \Phi_{l,4}^{(u)}\mathrm{Im}(\mathrm{X})}\right] \qquad (52)
\end{aligned}$$

where $\tilde{\mathrm{Z}}$ is a split vector which satisfies that $\mathrm{Z} = [\tilde{Z}_0, \tilde{Z}_1, \cdots, \tilde{Z}_{N-1}]^{\mathsf{T}} + j[\tilde{Z}_N, \tilde{Z}_{N+1}, \cdots, \tilde{Z}_{2N-1}]^{\mathsf{T}}$. We can rewrite (52) as

$$\mathrm{Z} = \Phi_{l,1}^{(u)}\mathrm{Re}(\mathrm{X}) + \Phi_{l,2}^{(u)}\mathrm{Im}(\mathrm{X}) + j\left\{\Phi_{l,3}^{(u)}\mathrm{Re}(\mathrm{X}) + \Phi_{l,4}^{(u)}\mathrm{Im}(\mathrm{X})\right\}. \tag{53}$$

Using the fact that $\Phi_{l,\kappa}^{(u)}, \kappa = 1,\cdots,4$ are X-matrices, we can derive that the ith and the $(N-i)$th entries of Z as follows. For $1 \le i \le \frac{N}{2} - 1$

$$\begin{aligned}
\mathrm{Re}(Z_i) =& \phi_{i,i}^1\mathrm{Re}(X_i) + \phi_{i,N-i}^1\mathrm{Re}(X_{N-i}) \\
&+ \phi_{i,i}^2\mathrm{Im}(X_i) + \phi_{i,N-i}^2\mathrm{Im}(X_{N-i}), \\
\mathrm{Im}(Z_i) =& \phi_{i,i}^3\mathrm{Re}(X_i) + \phi_{i,N-i}^3\mathrm{Re}(X_{N-i}) \\
&+ \phi_{i,i}^4\mathrm{Im}(X_i) + \phi_{i,N-i}^4\mathrm{Im}(X_{N-i}) \qquad (54a)
\end{aligned}$$

and

$$\begin{aligned}
\mathrm{Re}(Z_{N-i}) =& \phi_{N-i,i}^1\mathrm{Re}(X_i) + \phi_{N-i,N-i}^1\mathrm{Re}(X_{N-i}) \\
&+ \phi_{N-i,i}^2\mathrm{Im}(X_i) + \phi_{N-i,N-i}^2\mathrm{Im}(X_{N-i}), \\
\mathrm{Im}(Z_{N-i}) =& \phi_{N-i,i}^3\mathrm{Re}(X_i) + \phi_{N-i,N-i}^3\mathrm{Re}(X_{N-i}) \\
&+ \phi_{N-i,i}^4\mathrm{Im}(X_i) + \phi_{N-i,N-i}^4\mathrm{Im}(X_{N-i}), \qquad (54b)
\end{aligned}$$

where $\phi_{i,j}^{\kappa}$ is the (i,j) entry of $\Phi_{l,\kappa}^{(u)}, \kappa = 1,\cdots,4$[2]. Therefore, we have proved from (54) that two source symbols X_i and X_{N-i} share two subcarriers Z_i and Z_{N-i}. ■

Proof: $\mathrm{F}_l^{(u)}$ is an orthogonal matrix, i.e., $\mathrm{F}_l^{(u)^{-1}} = \mathrm{F}_l^{(u)^{\mathsf{T}}}$.

Using the definition of the JROF process, the inverse matrix of $\mathrm{R}_{\theta,m_l^{(u)}}$ in (11) is easily found as

$$\mathrm{R}_{\theta,m_l^{(u)}}^{-1} = \left[\begin{array}{c|c} \mathrm{I}\cos\theta & \mathrm{P}_{-m_l^{(u)}}\sin\theta \\ \hline -\mathrm{I}\sin\theta & \mathrm{P}_{-m_l^{(u)}}\cos\theta. \end{array}\right] \tag{55}$$

which satisfies $\mathrm{R}_{\theta,m_l^{(u)}}^{-1} = \mathrm{R}_{\theta,m_l^{(u)}}^{\mathsf{T}}$. If we note that product of orthogonal matrices is also orthogonal, it is induced that $\mathrm{G}_l^{(u)}$ is orthogonal matrix from (13). Therefore, we can see from (26) that $\mathrm{F}_l^{(u)}$ is an orthogonal matrix. ■

REFERENCES

[1] R. Chang and R. Gibby, "A theoretical study of performance of an orthogonal multiplexing data transmission scheme," *IEEE Trans. Commun. Technol.*, vol. 16, no. 4, pp. 529–540, Aug. 1968.

[2] S. Weinstein and P. Ebert, "Data transmission by frequency-division multiplexing using the discrete Fourier transform," *IEEE Trans. Commun. Technol.*, vol. 19, no. 5, pp. 628–634, Oct. 1971.

[2]For $\phi_{i,j}^{\kappa}$, both indices in $\Phi_{l,\kappa}^{(u)}$, l, and u are omitted for notation brevity.

[3] L. J. Cimini, Jr., "Analysis and simulation of a digital mobile channel using orthogonal frequency division multiplexing," *IEEE Trans. Commun.*, vol. 33, no. 7, pp. 665–675, Jul. 1985.
[4] T. Jiang and Y. Wu, "An overview: Peak-to-average power ratio reduction techniques for OFDM signals," *IEEE Trans. Broadcast.*, vol. 54, no. 2, pp. 257–268, Jun. 2008.
[5] R. O'Neill and L. Lopes, "Envelope variations and spectral splatter in clipped multicarrier signals," in *Proc. IEEE Int. Symp. Pers. Indoor and Mobile Radio Commun. (PIMRC)*, Toronto, Canada, Sep. 1995, pp. 71–75.
[6] X. Li and L. J. Cimini, Jr., "Effects of clipping and filtering on the performance of OFDM," *IEEE Commun. Lett.*, vol. 2, no. 5, pp. 131–133, May 1998.
[7] A. Jones, T. Wilkinson, and S. Barton, "Block coding scheme for reduction of peak to mean envelope power ratio of multicarrier transmission schemes," *Electron. Lett.*, vol. 30, no. 25, pp. 2098–2099, Dec. 1994.
[8] J. Davis and J. Jedwab, "Peak-to-mean power control and error correction for OFDM transmission using Golay sequences and Reed-Muller codes," *Electron. Lett.*, vol. 33, no. 4, pp. 267–268, Feb. 1997.
[9] K. Paterson, "Generalized Reed-Muller codes and power control in OFDM modulation," *IEEE Trans. Inf. Theory*, vol. 46, no. 1, pp. 104–120, Jan. 2000.
[10] J. Tellado, "Peak to average power reduction in multicarrier modulation," Ph.D. dissertation, Stanford Univ, Stanford, CA, 1999.
[11] B. Krongold and D. Jones, "PAR reduction in OFDM via active constellation extension," *IEEE Trans. Broadcast.*, vol. 49, no. 3, pp. 258–268, Sep. 2003.
[12] R. Bauml, R. Fischer, and J. Huber, "Reducing the peak-to-average power ratio of multicarrier modulation by selected mapping," *Electron. Lett.*, vol. 32, no. 22, pp. 2056–2057, Oct. 1996.
[13] S. Muller and J. Huber, "OFDM with reduced peak-to-average power ratio by optimum combination of partial transmit sequences," *Electron. Lett.*, vol. 33, no. 5, pp. 368–369, Feb. 1997.
[14] S. Muller and J. Huber, "A novel peak power reduction scheme for OFDM," in *Proc. IEEE Int. Symp. Pers. Indoor and Mobile Radio Commun. (PIMRC)*, Helsinki, Finland, Sep. 1997, vol. 3, pp. 1090–1094.
[15] L. J. Cimini, Jr. and N. Sollenberger, "Peak-to-average power ratio reduction of an OFDM signal using partial transmit sequences," *IEEE Commun. Lett.*, vol. 4, no. 3, pp. 86–88, Mar. 2000.
[16] S. H. Han and J. H. Lee, "PAPR reduction of OFDM signals using a reduced complexity PTS technique," *IEEE Signal Process. Lett.*, vol. 11, no. 11, pp. 887–890, Nov. 2004.
[17] A. Jayalath and C. Tellambura, "Adaptive PTS approach for reduction of peak-to-average power ratio of OFDM signal," *Electron. Lett.*, vol. 36, no. 14, pp. 1226–1228, Jul. 2000.
[18] T. Jiang, W. Xiang, P. Richardson, J. Guo, and G. Zhu, "PAPR reduction of OFDM signals using partial transmit sequences with low computational complexity," *IEEE Trans. Broadcast.*, vol. 53, no. 3, pp. 719–724, Sep. 2007.
[19] H. Breiling, S. H. Muller-Weinfurtner, and J. B. Huber, "SLM peak-power reduction without explicit side information," *IEEE Commun. Lett.*, vol. 5, no. 6, pp. 239–241, Jun. 2001.
[20] Z. Du, N. Beaulieu, and J. Zhu, "Selective time-domain filtering for reduced-complexity PAPR reduction in OFDM," *IEEE Trans. Veh. Technol.*, vol. 58, no. 3, pp. 1170–1176, Mar. 2009.
[21] L. Guan, T. Jiang, D. Qu, and Y. Zhou, "Joint channel estimation and PTS to reduce peak-to-average-power radio in OFDM systems without side information," *IEEE Signal Process. Lett.*, vol. 17, no. 10, pp. 883–886, Oct. 2010.
[22] G. Lu, P. Wu, and D. Aronsson, "Peak-to-average power ratio reduction in OFDM using cyclically shifted phase sequences," *IET Commun.*, vol. 1, no. 6, pp. 1146–1151, Dec. 2007.
[23] E. Alsusa and L. Yang, "A low-complexity time-domain linear symbol combining technique for PAPR reduction in OFDM systems," *IEEE Trans. Signal Process.*, vol. 56, no. 10, pp. 4844–4855, Oct. 2008.
[24] C. Tellambura, "Computation of the continuous-time PAR of an OFDM signal with BPSK subcarriers," *IEEE Commun. Lett.*, vol. 5, no. 5, pp. 185–187, May 2001.
[25] C. Li, T. Jiang, Y. Zhou, and H. Li, "A novel constellation reshaping method for PAPR reduction of OFDM signals," *IEEE Trans. Signal Process.*, vol. 59, no. 6, pp. 2710–2719, Jun. 2011.
[26] L. Yang and E. Alsusa, "Novel low-complexity post-IFFT PAPR reduction technique for OFDM systems," in *Proc. IEEE Wireless Commun. Netw. Conf. (WCNC)*, Las Vegas, NV, Apr. 2006, pp. 2006–2011.
[27] L. Yang and E. Alsusa, "Novel low-complexity post-IFFT PAPR reduction technique by utilising amplitude transforming for OFDM systems," in *Proc. IEEE Wireless Commun. Netw. Conference (WCNC)*, Kowloon, Mar. 2007, pp. 1339–1343.
[28] C. Rapp, "Effects of HPA-nonlinearity on 4-DPSK-OFDM-signal for a digital sound broadcasting system," in *Proc. 2nd Eur. Conf. Satellite Commun.*, Liege, Belgium, Oct. 1991, pp. 179–184.
[29] J. R. Schott, *Matrix Analysis for Statistics*, 2nd ed. New York: Wiley, 2004.

Seung-Sik Eom (S'06) received the B.S. and M.S. degrees in electrical engineering from Korea University, Seoul, in 2005 and 2007, respectively. He is currently working toward the Ph.D. degree at the School of Electrical Engineering, Korea University. His current research interest is signal processing in OFDM systems including PAPR reduction schemes with low complexity.

Haewoon Nam (S'99–M'07–SM'11) received the B.S. degree in electrical communication engineering from Hanyang University, Seoul, Korea, in 1997, the M.S. degree in electrical engineering from Seoul National University, Seoul, Korea, in 1999, and the Ph.D. degree in electrical and computer engineering from the University of Texas at Austin in 2006.

From February 1999 to July 2002, he was with Samsung Electronics, where he was engaged in the design and development of CDMA and GSM/GPRS baseband modem processors. In summer 2003, he was with the IBM T.J. Watson Research Center, Yorktown Heights, NY, and in fall 2005, he was with Freescale Semiconductor. His industry experience also includes work at Samsung Advanced Institute of Technology. In October 2006, he joined the Mobile Devices Technology Office, Motorola Inc., Austin, where he was involved in algorithm design and development of 3GPP LTE modem processor. Later in 2010, he was with Apple Inc., Cupertino, CA, where he worked on research and development of next-generation smart mobile systems. Since March 2011, he has been with the department of electronics and communication engineering, Hanyang University, where he is an Assistant Professor.

He is a recipient of the Korean government overseas scholarship in the field of electrical engineering.

Young-Chai Ko (S'97–M'01–SM'06) received the B.Sc. degree in electrical and telecommunication engineering from the Hanyang University, Seoul, Korea, and the M.S.E.E. degree and the Ph.D. degree in electrical engineering from the University of Minnesota, Minneapolis, in 1999 and 2001, respectively.

In March 2001, he joined Texas Instruments, Inc., San Diego Wireless Center, San Diego, CA, where he worked on WCDMA MODEM system design. Since March 2004, he has been with School of Electrical Engineering at Korea University where he is currently an Associate Professor and the Director of High-Speed Human Interface Center (H2IC) supported by Samsung Electro-Mechanics. His research focus is on the performance analysis and the design of wireless communication systems in the physical layer.